

# Combinatorial Control of Human RNA Polymerase II (RNAP II) Pausing and Transcript Cleavage by Transcription Factor IIF, Hepatitis $\delta$ Antigen, and Stimulatory Factor II\*

Received for publication, July 15, 2003, and in revised form, September 2, 2003  
Published, JBC Papers in Press, September 23, 2003, DOI 10.1074/jbc.M307590200

Chunfen Zhang, Honggao Yan, and Zachary F. Burton $\ddagger$

From the Department of Biochemistry and Molecular Biology, Michigan State University,  
East Lansing, Michigan 48824-1319

**When RNA polymerase II (RNAP II) is forced to stall, elongation complexes (ECs) are observed to leave the active pathway and enter a paused state. Initially, ECs equilibrate between active and paused conformations, but with stalls of a long duration, ECs backtrack and become sensitive to transcript cleavage, which is stimulated by the EC rescue factor stimulatory factor II (TFIIS/SII). In this work, the rates for equilibration between the active and pausing pathways were estimated in the absence of an elongation factor, in the presence of hepatitis  $\delta$  antigen (HDAG), and in the presence of transcription factor IIF (TFIIF), with or without addition of SII. Rates of equilibration between the active and paused states are not very different in the presence or absence of elongation factors HDAG and TFIIF. SII facilitates escape from stalled ECs by stimulating RNAP II backtracking and transcript cleavage and by increasing rates into and out of the paused EC. TFIIF and SII cooperate to merge the pausing and active pathways, a combinatorial effect not observed with HDAG and SII. In the presence of HDAG and SII, pausing is observed without stimulation of transcript cleavage, indicating that the EC can pause without backtracking beyond the pretranslocated state.**

Our laboratory has applied transient state kinetic analysis (1–3) to probe the mechanism and regulation of elongation by human RNA polymerase II (RNAP II)<sup>1</sup> (4, 5). In the current work, we concentrate on control of the branch point between the active synthesis pathway and the pausing pathway. We measure the rate by which RNAP II leaves the active synthesis pathway to enter the pausing pathway after encountering a barrier to elongation caused by withholding the next substrate nucleoside triphosphate.

It has been suggested that transcription factor IIF (TFIIF) stimulates RNAP II elongation by suppressing transcriptional pausing (6–8). TFIIF is a general initiation and elongation

factor for RNAP II, composed of RAP74 and RAP30 subunits (RAP for RNA polymerase II-associating protein). *In vitro*, TFIIF stimulates elongation about 5–10-fold, achieving rates on chromatin-free DNA templates that are similar to rates observed on chromatinized templates *in vivo* (6–12). Based on transient state kinetic studies, our laboratory recently proposed a mechanism for RNAP II elongation stimulated by TFIIF and hepatitis  $\delta$  antigen (HDAG) (5). We have also demonstrated the major defects of the RAP74 I176A mutant in general and transient state elongation assays, providing insight into the functions of TFIIF in the RNAP II mechanism (11). We find that TFIIF exerts a global effect on elongation. TFIIF helps commit elongation complexes (ECs) to the forward synthesis pathway. TFIIF stimulates the rate of chemistry and accelerates a slow step after chemistry in the normal processive transition between bonds, a step that includes translocation and pyrophosphate release (5, 11). We conjecture that TFIIF binds to an external surface of RNAP II, tightens the RNAP II clamp, which grasps the RNA-DNA hybrid, and optimizes conditions for chemistry during elongation. Furthermore, in the presence of TFIIF, RNAP II utilizes the incoming NTP substrate to drive translocation of the RNA-DNA hybrid past the RNAP II active site (5).

The small RNA genome of hepatitis  $\delta$  virus (HDV) is packaged and mobilized as a satellite particle by hepatitis B virus (13–15). HDAG is the sole gene product of HDV. HDAG participates in HDV replication, in part by stimulating ribozyme activities of HDV RNA (16, 17). Recently, however, HDAG was shown to be a potent stimulator of elongation by RNAP II (5, 18, 19). In the viral life cycle, HDAG is thought to stimulate HDV replication and transcription by helping to convert cellular RNAP II from a DNA template-directed RNAP to an RNA template-directed RNAP that can recognize the HDV genome (20–22). Because HDV replication and transcription are not yet fully recapitulated using *in vitro* systems (18, 23), our laboratory has pursued studies of HDAG stimulation of RNAP II using DNA templates (5, 18). In the presence of HDAG, the RNAP II elongation mechanism is significantly altered (5). Compared with TFIIF, HDAG reduces the NTP dependence of a slow step that occurs after chemistry. We speculate that this slow step represents a *taut*  $\rightarrow$  *relaxed* conformational change in RNAP II that loosens contact with the newly polymerized RNA base and facilitates subsequent release of pyrophosphate. This conformational change might be attributed to a loosening of the RNAP II clamp, and HDAG may regulate the tightness of clamp closure (5). Loosening the clamp could contribute to the switch in specificity required for RNAP II to replicate and transcribe the HDV RNA template. In the TFIIF-stimulated mechanism the *taut*  $\rightarrow$  *relaxed* transition after chemistry is coupled to NTP-driven translocation. In the HDAG-stimulated mecha-

\* This work was supported in part by National Institutes of Health Grant GM57461 (to Z. F. B.). The costs of publication of this article were defrayed in part by the payment of page charges. This article must therefore be hereby marked "advertisement" in accordance with 18 U.S.C. Section 1734 solely to indicate this fact.

$\ddagger$  Recipient of support from the Michigan State University Agricultural Experiment Station. To whom correspondence should be addressed: Dept. of Biochemistry and Molecular Biology; Michigan State University, E. Lansing, MI 48824-1319. Tel.: 517-353-0859; Fax: 517-353-9334; E-mail: burton@msu.edu.

<sup>1</sup> The abbreviations used are: RNAP II, RNA polymerase II; EC, elongation complex; HDAG, hepatitis  $\delta$  antigen; TFIIF, transcription factor IIF; TFIIS/SII, transcription factor, RNAP II, stimulatory/stimulatory factor II; HDV, hepatitis  $\delta$  virus.

nism, the *taut* → *relaxed* transition does not depend on translocation and is instead followed by NTP-driven translocation. TFIIF and HDAG, therefore, stimulate the same basic RNAP II mechanism but regulate the order of key events (translocation and relaxation of the active site), perhaps by regulating the extent and quality of clamp closure.

TFIIS/SII is a general elongation factor known to rescue stalled and arrested ECs (24–29). SII is a functional analogue of eubacterial Gre transcription factors (30, 31). During backtracking, the RNAP II active site slips off the 3' end of the RNA chain and scans 3' → 5' along the RNA within the RNA-DNA hybrid. Backtracked RNA, which extrudes through the RNAP secondary pore, can be cross-linked to SII and to Gre factors (30, 32, 33). SII stimulates an intrinsic RNA cleavage activity attributed to the RNAP II active site, as indicated by the  $\alpha$ -amanitin sensitivity and  $Mg^{2+}$  dependence of the cleavage reaction (28, 34, 35). Recently, the roles of SII and Gre factors were substantially clarified by x-ray and electron microscopy structural studies demonstrating SII and GreB bound to their respective RNAPs (36, 37). SII and Gre factors penetrate the secondary pore of target RNAPs projecting a bound  $Mg^{2+}$  atom into the RNAP active site. The  $Mg^{2+}$  atom held by SII or GreB is poised to participate with a second  $Mg^{2+}$  atom within the RNAP catalytic center to cleave the nascent RNA chain. SII binding significantly rearranges the conformation of the RNAP II active site and the environment of the RNA-DNA hybrid, indicating that some functions of SII may be mediated by allosteric effects. SII is not observed to strongly stimulate forward synthesis by RNAP II (6, 7), so the extent to which SII might participate in forward RNA synthesis is not known.

In this paper, we have probed the RNAP II pausing mechanism in the presence of TFIIF, HDAG, and SII, added separately or in combination. We demonstrate combinatorial control of pausing by SII and TFIIF. SII cooperates with TFIIF to merge the RNA synthesis and pausing pathways, resulting in acceleration of rates into and out of the pausing pathway. In contrast, SII and HDAG do not cooperate in this way. Judging from the combinatorial effects of SII and HDAG, the paused EC is unlikely to be backtracked beyond the pretranslocated state, because in the presence of HDAG the paused EC resists SII-mediated transcript cleavage. Under elongation conditions, SII stimulates RNA cleavage primarily in dinucleotide increments (28, 35, 38, 39). When paused ECs backtrack by a single base from the pretranslocated state, the RNAP II active site is poised for SII-stimulated RNA cleavage, and HDAG may therefore resist cleavage by inhibiting backtracking.

#### EXPERIMENTAL PROCEDURES

**Cell Culture, Extracts, and Proteins**—HeLa cells were purchased from the National Cell Culture Center (Minneapolis, MN). Extracts of HeLa cell nuclei were prepared as described (40). Recombinant HDAG (18) and TFIIF (41, 42) were prepared as described.

**Rapid Quench Elongation Experiments**—Detailed protocols for rapid quench-flow experiments have been published previously (4, 5, 11). Briefly,  $^{32}P$ -labeled C40 (40-nucleotide RNA ending in a 3'-CMP) RNAP II ECs were formed on metal bead-immobilized templates in a HeLa transcription extract. Initiation was from the adenovirus major late promoter using a modified downstream sequence ( $^1ACTCTCTCCCTCTCTCTCTCTCTCTCCCTCC^{40}$ ). The purpose of the 39-nucleotide CT cassette was to synthesize C40 with ApC dinucleotide, dATP, [ $\alpha$ - $^{32}P$ ]CTP, and UTP, bypassing the requirement for ATP and GTP. C40 ECs were washed with 1% Sarkosyl and 0.5 M KCl buffer to dissociate initiation, elongation, pausing, and termination factors, contributed by the HeLa extract, and re-equilibrated with transcription buffer containing 8 mM  $MgCl_2$  and 20  $\mu M$  CTP and UTP. Elongation factors were added as indicated in the experimental protocols. Subsequent steps were performed using the Kintek Rapid Chemical Quench-Flow (RQF-3) instrument. Most experiments were done with the instrument operated in pulse-chase mode. Elongation was through the sequence  $^{40}CAAAGGCC^{47}$ . ATP (added through the right sample port)

was added to C40 ECs (left sample port) in a timed pulse (0.01–240 s), followed by a GTP chase, added through the middle syringe (normally the quench syringe). Reactions were quenched as samples were expelled from the RQF-3 into collection tubes containing 0.5 M EDTA. By using the 3-syringe sample mixing chamber, the shortest possible time of the GTP chase was determined by the length of the RQF-3 exit line. We calibrated the shortest chase time to be 0.045 s. Longer chase times were obtained by a programmed delay, holding the sample in the exit line before expulsion into quench solution. The experiment shown in Fig. 6 was done with the RQF-3 run in the standard reaction mode. A 30-s ATP pulse was done on the bench top followed by EC transfer into the left sample port. GTP was added from the right sample port, and samples were quenched after various times, as described (4, 5, 11).

**Kinetic Modeling**—Kinetic models were fit to experimental data using the program KinTekSim (43, 44). No ATP- or GTP-dependent steps were considered in these models, because elongation from C40 was found to be largely independent of the ATP concentration, within a large concentration range (10–250  $\mu M$  ATP), and modeling ATP-dependent steps was not necessary. GTP-dependent effects were also neglected, because high GTP concentrations were analyzed, and GTP chase times were selected that allowed fairly complete conversion of active pathway A43 ECs to G44 and longer products.

Model-independent analysis (45, 46) was done with the program Microcal Origin version 6.1, fitting rate data to single, double, or triple exponential rate curves, as appropriate.

#### RESULTS

In previous work, we indicated that stalled RNAP II ECs tend to revert to the pretranslocated state (5), consistent with the yeast RNAP II EC structure, which is found primarily in the pretranslocated conformation (47). We also noted that stalling induces transcriptional pausing, because the efficiency of rapid elongation from the stall site was highest with the shortest stall times, showing that the longer the stall time, the more ECs would pause (4). This trend toward pausing, however, was only observed for a few seconds, after which time a steady state condition was established in which the efficiency of elongation remained constant for several minutes. We interpreted this observation to mean that the pausing and active synthesis pathways could assume a dynamic equilibrium that required 1–10 s to establish but would remain stable for minutes before the EC would enter backtracked and arrested elongation modes.

**Kinetics of Stalling and Entry into the Paused EC**—In the current work, we measure the efficiency of rapid RNAP II elongation from a stall position as a function of stall time. Extending the RNA through the sequence  $^{40}CAAAGG^{45}$ , RNAP II ECs were advanced from C40 to A43, by addition of 200  $\mu M$  ATP (Fig. 1). After variable times of stalling from 0.25 to 240 s, 250  $\mu M$  GTP was added, and after a 0.55-s elongation time, reactions were quenched with EDTA. The GTP chase time was selected because 0.55 s was sufficient to extend activated A43 ECs to G44 or longer positions, but the paused A43 ECs were not extended (5, 11). Because a 0.55-s GTP chase was necessary to sample the distribution of active and paused ECs, the time resolution of this experiment is somewhat limited, but the rates that we measure are slow enough that this is not a severe complication. A further difficulty is that, because of slow escape from C40, not all C40 ECs can be delivered to the A43 position rapidly. A43 and longer products are only detected after about 1 s, so resolution on the time axis is limited to about 1.5 s. By considering only those ECs that reach A43 or longer positions, however, this experimental difficulty was largely overcome. The efficiency of elongation from A43 is defined as  $G44+/A43+$ , in which  $G44+$  includes G44 plus all longer transcripts and  $A43+$  includes A43 plus all longer transcripts. By doing the calculation based on efficiency, ECs that do not advance from C40 to A43 are neglected in the analysis and do not compromise the estimation of the equilibration rate. To an extent, this analysis is complicated because A43 ECs are continually form-

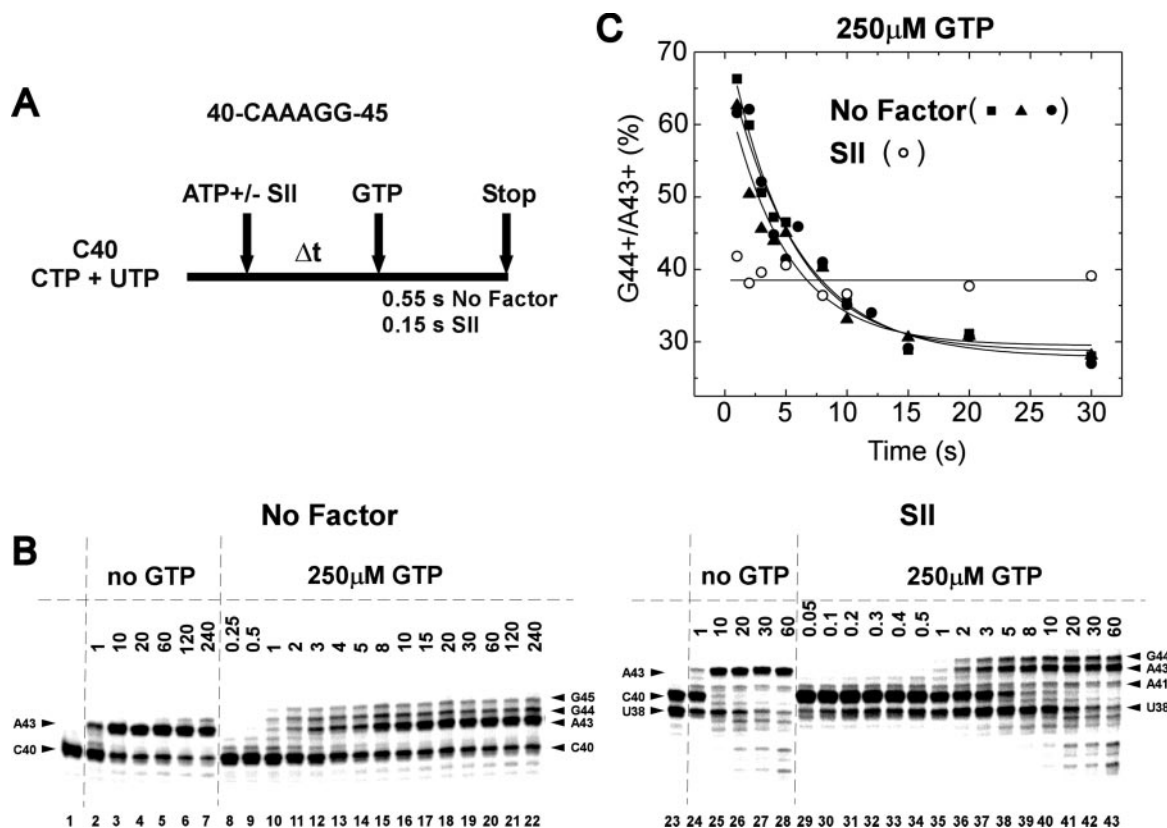


FIG. 1. Exit of the RNAP II EC from the activated elongation state in the absence or presence of SII. *A*, reaction protocol and RNA sequence. ECs were stalled at the A43 position for different times followed by a brief chase with 250  $\mu$ M GTP. *B*, RNAP II elongation in the absence of an elongation factor (left panel) or in the presence of SII (right panel). Lanes 1 and 23, no ATP or GTP addition; lanes 2–7 and 24–28, 200  $\mu$ M ATP pulse but no GTP chase; lanes 8–22 and 29–43, ATP pulse followed by a 250  $\mu$ M GTP chase for 0.55 (–SII) or 0.15 s (+SII). ATP pulse times are in seconds. *C*, plots of elongation efficiency (G44+/A43+) percent versus ATP pulse time in seconds. Data are fit to single exponential rate curves. Rates for entering the paused state are  $k_e = 0.18 \pm 0.03$ ,  $0.21 \pm 0.03$ , and  $0.19 \pm 0.03$  s $^{-1}$  in three independent experiments ( $\pm$  S.E.) (Table D). In the presence of SII, the rate of equilibration between the active and the paused states could not be measured. The C40 control reaction shown in *B*, lane 23, was treated for a few seconds on the bench top with SII before quenching with EDTA. In lanes 29–43, the time of SII exposure varies with the time of the ATP pulse.

ing throughout the course of the reaction, and the stall time is therefore somewhat variable for different A43 ECs. The rates we estimate therefore are likely to be a slight underestimate of the true value, because the dwell time at A43 is slightly shorter than the time of the ATP pulse. There is, however, no better experimental means to measure the rates of equilibration between the activated and the paused state, because the reaction cannot commence with a completely synchronous population of active pathway A43 ECs.

Despite these limitations, the observed decrease in elongation efficiency as a function of the ATP pulse time (Fig. 1, *B* and *C*) can be described by a single-phase exponential curve and a first-order apparent rate, indicating that the rate for equilibration of the active synthesis and pausing pathways can be estimated by this method. Fig. 1*B* shows RNAP II elongation in the absence (lanes 1–22) and presence of SII (lanes 23–43). Fig. 1*C* shows PhosphorImager quantitation of the data shown in Fig. 1*B*, along with data from two replicate experiments, to estimate the kinetics of pausing. Fitting the data to single exponential curves, the rate of equilibration between the active and pausing pathways was estimated as  $k_e = 0.18 \pm 0.03$ ,  $0.21 \pm 0.03$ , and  $0.19 \pm 0.03$  s $^{-1}$  ( $k_e$  for rate of equilibration; errors are reported as standard error). The rate  $k_e$  for equilibration of the system should be equal to  $k_p + k_{-p}$  (rate constants into and out of the paused EC). Values for  $k_e$ ,  $k_p$ , and  $k_{-p}$  for the entire paper are shown in Table I.

As controls, samples were run with an ATP pulse from 1 to 240 s without a GTP chase (Fig. 1*B*, lanes 2–7). Very little background GMP incorporation is detected, even with a 240-s

pulse, indicating that there is little GTP contamination in the ATP used in the pulse and that misincorporation of AMP for GMP is not significant during the time course of the experiment.

*Effects of TFIIS/SII on Pausing and Transcript Cleavage*—Because SII regulates RNAP II arrest and transcript cleavage, an experiment was done with addition of SII to determine whether SII regulates pausing by RNAP II. In the absence of other elongation factors, however, we found that, when preincubated with the RNAP II EC, SII was very aggressive in stimulating backtracking and cleavage of the stalled C40 EC (experiment not shown). The C40 EC was not stable, even though during the preincubation reactions contain 20  $\mu$ M CTP and UTP, which should allow cleaved ECs to re-extend to the C40 position. In order to compare RNAP II elongation  $\pm$  SII, SII was added at the same time as ATP, making the time of SII addition variable along with the time of EC stalling at A43. In the experiment shown, the GTP chase time was 0.15 s, but results were similar with a chase time of 0.55 s (not shown). SII is functional in this assay, because it stimulates dinucleotide cleavage from C40  $\rightarrow$  U38, from U38 to smaller RNAs, and from A43  $\rightarrow$  A41. SII allows for pausing at A43, because the majority of transcripts that reach A43 do not extend to G44 with a 0.15- or 0.55-s GTP chase time, and these chase times are sufficient for active pathway ECs to advance (5, 11). However, the rates in and out of the paused state can no longer be resolved because the efficiency of elongation from A43 is not observed to change with time of stalling at A43 (Fig. 1*B* (lanes 36–43) and Fig. 1*C* (open symbols)). Paused and active A43 ECs appear to have

TABLE I  
Values for  $k_e$ ,  $k_p$ , and  $k_{-p}$

Factors	-SII			+SII		
	$k_e$	$k_p$	$k_{-p}$	$k_e$	$k_p$	$k_{-p}$
	$s^{-1}$	$s^{-1}$	$s^{-1}$	$s^{-1}$	$s^{-1}$	$s^{-1}$
No factor	0.18 ± 0.03 0.21 ± 0.03 0.19 ± 0.03	0.14	0.05	>1.7	2.6	0.95
HDAG	0.32 ± 0.02 0.29 ± 0.02 0.28 ± 0.02	0.11	0.07	0.64 ± 0.11	0.33	0.37
TFIIF	0.19 ± 0.01 0.18 ± 0.01 0.21 ± 0.01	0.096	0.10	>14	ND <sup>a</sup>	ND <sup>a</sup>

<sup>a</sup> ND, not determined.

equilibrated within at least 2 s, so 2 s might represent about  $5 \times t_{1/2}$  of the rate of equilibration between active synthesis and pausing. Based on this estimate, the rate of equilibration should be faster than  $1.7 \text{ s}^{-1}$ . Therefore, SII may accelerate rates into and out of the pausing pathway. On the other hand, some of the apparent effect of SII on pausing might rather be attributed to an effect of SII on transcript cleavage. SII stimulation of RNA cleavage could shorten the time of stalling at the A43 position, so apparent acceleration of rates into and out of the paused state might reflect rapid cleavage and re-extension of ECs to the A43 position, before GTP addition to the reaction. In any event, we conclude that EC pausing occurs in the presence of SII, although these paused RNAP II ECs are very sensitive to SII-stimulated cleavage.

**Effects of HDAG on Transcriptional Pausing**—The rate of equilibration between the active and pausing pathways was then estimated in the presence of the viral elongation factor HDAG (Fig. 2). In part, this experiment was done to determine whether enhancement of elongation rates by HDAG could be attributed to blocking entry into the deeply paused RNAP II EC. As in the absence of a stimulatory factor, in the presence of HDAG, the efficiency of extension from A43→G44 and longer products was observed to decrease as a function of stall time at A43. This conclusion is indicated by inspection of gel data (Fig. 2B, lanes 8–23), because the A43 band continues to increase in intensity compared with the G44 and G45 bands, as stall time increases. The 200  $\mu\text{M}$  ATP pulse was from 0.1 to 60 s. In the presence of HDAG, most C40 ECs advance within 1–1.5 s, so the rate of escape from C40 is faster, and the synchrony of forming A43 ECs is much better in the presence of HDAG than in the absence of a stimulatory elongation factor (compare Figs. 1 and 2). The chase time with 250  $\mu\text{M}$  GTP was 0.045 s, which was deemed sufficient to convert most activated A43 ECs but not paused A43 ECs to G44 or G45 (5). From PhosphorImager quantitation, the efficiency of A43 EC extension to G44 and longer products was observed to decrease with longer stall times at A43 (Fig. 2, B, lanes 10–23, and C). Because the efficiency of elongation from A43 decreased as the dwell time at A43 increased, A43 ECs must be entering a paused state, whether or not the 0.045-s GTP chase time for A43→G44 elongation is sufficient to extend all poised A43 ECs. Little background GMP incorporation or AMP misincorporation is detected with a 60-s ATP pulse time (Fig. 2B, lane 7). The rate of equilibration between the active and pausing pathways is estimated as  $k_e = 0.32 \pm 0.02$ ,  $0.29 \pm 0.02$ , and  $0.28 \pm 0.02 \text{ s}^{-1}$ , in three independent determinations (Table I). As above,  $k_e = k_p + k_{-p}$ . Although differences between these rates and those observed in the absence of an elongation factor appear statistically significant, HDAG appears to *increase* the rate of entering the paused state. HDAG is a stimulatory elongation factor, but speeding up the rate into the paused state would slow

elongation. Furthermore, the 30% difference in rates appears too small to strongly influence the most rapid elongation rates.

**Antagonistic Effects of HDAG and SII**—An important question to ask about paused ECs is the extent to which they are backtracked. SII is a probe for backtracked ECs because SII stimulates cleavage and subsequent re-start from a shortened transcript 3' end. Under elongation conditions, SII primarily stimulates cleavage of dinucleotides (27, 28, 35, 38). It is not known whether SII can stimulate backtracking of the RNAP II EC or the extent to which the paused EC is backtracked. If paused A43 ECs become backtracked by a single nucleotide from the pretranslocated state, significant A43→A41 cleavage is expected in the presence of SII, because backtracking of one nucleotide from the pretranslocated EC orients the RNAP II active site for dinucleotide cleavage. Because in the presence of HDAG and SII deep pausing is observed without stimulation of SII-mediated cleavage (Fig. 2B, lanes 26–29 and 38–44), the RNAP II EC can enter a paused state, without stimulation of RNA cleavage. HDAG modifies the paused A43 EC so that it remains relatively insensitive to SII, indicating that the paused EC may not be backtracked beyond the pretranslocated state. Above, we showed that in the absence of HDAG the paused EC was highly sensitive to backtracking and cleavage with addition of SII (compare Figs. 1 and 2). The RNAP II EC, therefore, appears to enter the paused state in a pretranslocated conformation and not a backtracked conformation (unless the pretranslocated state is considered to be backtracked by 1 nucleotide). SII appears to stimulate the transition between the paused state and the backtracked state, in the absence of another elongation factor (Fig. 1), but, in the presence of HDAG, SII-stimulated backtracking and RNA cleavage are suppressed (Fig. 2).

In the absence of another elongation factor, SII may increase rates into and out of the paused state at A43, although this observation may be partly attributable to effects of SII on transcript cleavage. In the presence of HDAG, however, SII appears to have a moderate effect on pausing. In Fig. 2B (lanes 36–44), pausing is clearly evident in the presence of both HDAG and SII. The estimated rate for equilibration with the pausing pathway is  $k_e = 0.64 \pm 0.11 \text{ s}^{-1}$ , so SII may slightly accelerate this rate (Table I). This conclusion is not certain, because SII stimulates RNA cleavage and therefore may reduce the time of EC stalling at the A43 position, although HDAG does resist SII-mediated transcript cleavage. SII is active in the reaction with HDAG, as indicated by enhanced cleavage of C40→U38 (Fig. 2B, lanes 24–26 and 30–39). Furthermore, increasing the SII concentration 10-fold (data not shown) had no significant effect on pausing in the presence of HDAG, although observed dinucleotide cleavage from C40→U38 and A43→A41 was enhanced by the increase in SII concentration. We conclude that the A43 EC is sensitive to effects of SII but that HDAG modifies the EC so that it becomes resistant to SII-mediated transcript cleavage. Furthermore, the major fraction of paused A43 ECs shows no evidence of being backtracked beyond the pretranslocated state. It appears from this result that the A43 EC can enter a paused state without backtracking, indicating that pausing is initially a conformational change in the EC. Backtracking appears to be an additional step, in which the RNAP II active site loses contact with the 3'-OH of the nascent RNA and scans 3' → 5' over the RNA within the RNA-DNA hybrid (see "Discussion").

**Suppression of Pausing by TFIIF**—TFIIF stimulates rates of elongation by RNAP II, at least in part, by suppressing transcriptional pausing (6–8, 12), so we wondered whether TFIIF could block exit from the active to the paused elongation pathway. The data in Fig. 3, however, indicate that blocking exit

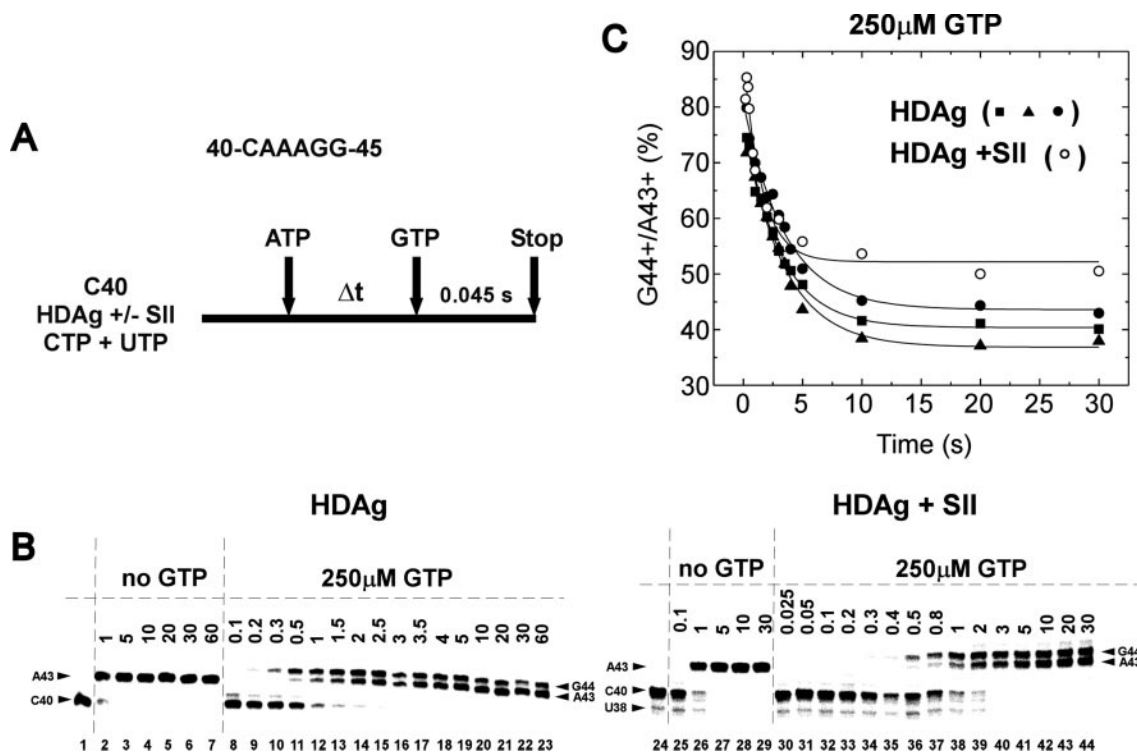


**FIG. 2. HDAG resists SII-mediated transcript cleavage.** *A*, reaction protocol and RNA sequence. ECs were extended to the A43 position for different times followed by a 0.045-s chase with 250  $\mu$ M GTP. *B*, HDAG-stimulated elongation in the absence of SII (*left panel*) or in the presence of SII (*right panel*). *Lanes 1 and 24*, no ATP pulse, no GTP chase; *lanes 2–7 and 25–29*, 200  $\mu$ M ATP pulse but no GTP chase; *lanes 8–23 and 30–44*, 200  $\mu$ M ATP pulse and 250  $\mu$ M GTP chase, added for 0.045 s. *C*, plots of elongation efficiency percent versus ATP pulse time in seconds. Rates for equilibration of the active and the paused states are  $k_e = 0.32 \pm 0.02$ ,  $0.29 \pm 0.02$ , and  $0.28 \pm 0.02$   $s^{-1}$  in three independent experiments. In the presence of SII, the rate for entering the paused state is  $k_e = 0.64 \pm 0.11$   $s^{-1}$  (Table I).

from the activated A43 EC to the paused EC cannot account for TFIIF-mediated stimulation of elongation. For some experiments, 50  $\mu$ M ATP, rather than 200  $\mu$ M ATP, was added in the ATP pulse to extend C40 ECs to A43. The ATP concentration was reduced because, in the presence of TFIIF, the EC can be highly poised for elongation, and traces of GTP can be scavenged to incorporate GMP, even when no GTP has been deliberately added to the reaction. Doing the experiment with a 200  $\mu$ M ATP pulse (not shown), instead of a 50  $\mu$ M ATP pulse, did not influence the rate determination but appeared to increase background GMP incorporation. In any event, the level of background GMP incorporation from the ATP pulse is not high enough to affect the results of the pausing rate determination.

In the presence of TFIIF, most C40 ECs are extended to A43 within 1.5–2 s. The efficiency of elongation from A43 appears to decrease until about 8 s, before the system approaches steady state balance between the active and paused pathways. The apparent rate of equilibration between the activated and the paused EC is  $k_e = 0.19 \pm 0.01$ ,  $0.18 \pm 0.01$ , and  $0.21 \pm 0.01$   $s^{-1}$ , in three independent determinations (Table I). The difference between these values and the values determined in the absence of an elongation factor was not statistically significant, so from this comparison TFIIF did not appear to directly block exit from the active elongation pathway into the paused state. We concluded that TFIIF blocks pausing during rapid elongation by influencing steps that are further along the active synthesis pathway.

**Combinatorial Pause Suppression by TFIIF and SII**—When SII is combined with TFIIF-stimulated RNAP II ECs, the efficiency of the forward reaction is strongly enhanced and pausing is suppressed at A43 (Fig. 3, *B* compare *left* and *right panels*, *C*). In the presence of SII, with the 250  $\mu$ M GTP chase, >75% of total ECs were extended to G44 and G45 in 0.045 s (Fig. 3, *B*, *right panel*, *C*), in contrast to a lower yield and (generally) a

lower efficiency in the absence of SII (Fig. 3, *B*, *left panel*, *C*). Furthermore, the efficiency of elongation from A43 was not observed to change as a function of stall time at A43 (Fig. 3C, *open symbols*). Apparently, in the presence of both TFIIF and SII, rates into and out of the paused state are too rapid to be measured within the time resolution (0.25 s) of the experiment. We conclude that TFIIF and SII cooperate to accelerate rates into and out of the RNAP II pausing pathway. Assuming that 0.25 s represents  $>5 \times t_{1/2}$ , the rate of equilibration with the pausing pathway must be faster than  $14$   $s^{-1}$  in the presence of both TFIIF and SII (Table I). This is a much faster rate than observed in the presence of both HDAG and SII ( $0.64$   $s^{-1}$ ), so TFIIF and SII cooperate to suppress pausing by RNAP II in a way that HDAG and SII do not.

Rates of RNA transcript cleavage and rates of backtracking are not yet known, so the 25% of ECs that remain at A43 after the 0.045 s chase could be: 1) poised for active synthesis but not yet extended, 2) paused, or 3) backtracked but not yet cleaved to A41. The 0.045-s 250  $\mu$ M GTP chase is sufficient for extension of most active pathway ECs (5). Furthermore, the fraction of RNAP II ECs that remains stalled at A43 requires a much longer chase time to advance (see Fig. 6, below). The only indication that ECs pause in the presence of both SII and TFIIF is that there is evidence of backtracking and cleavage from the A43 position (A43 $\rightarrow$ A41), which indicates a paused intermediate into the backtracked state. If remaining A43 ECs are primarily backtracked but not yet cleaved, the rate of SII-stimulated RNA cleavage must be slow. Furthermore, detection of A41 in the presence of 50  $\mu$ M ATP indicates that resumption of elongation after RNA cleavage also is slow, requiring a recovery period before active synthesis can resume.

**Kinetic Modeling of Equilibration between the Active and Pausing Pathways**—Although our estimations of rates of equilibration with the pausing pathway provided precise measure-

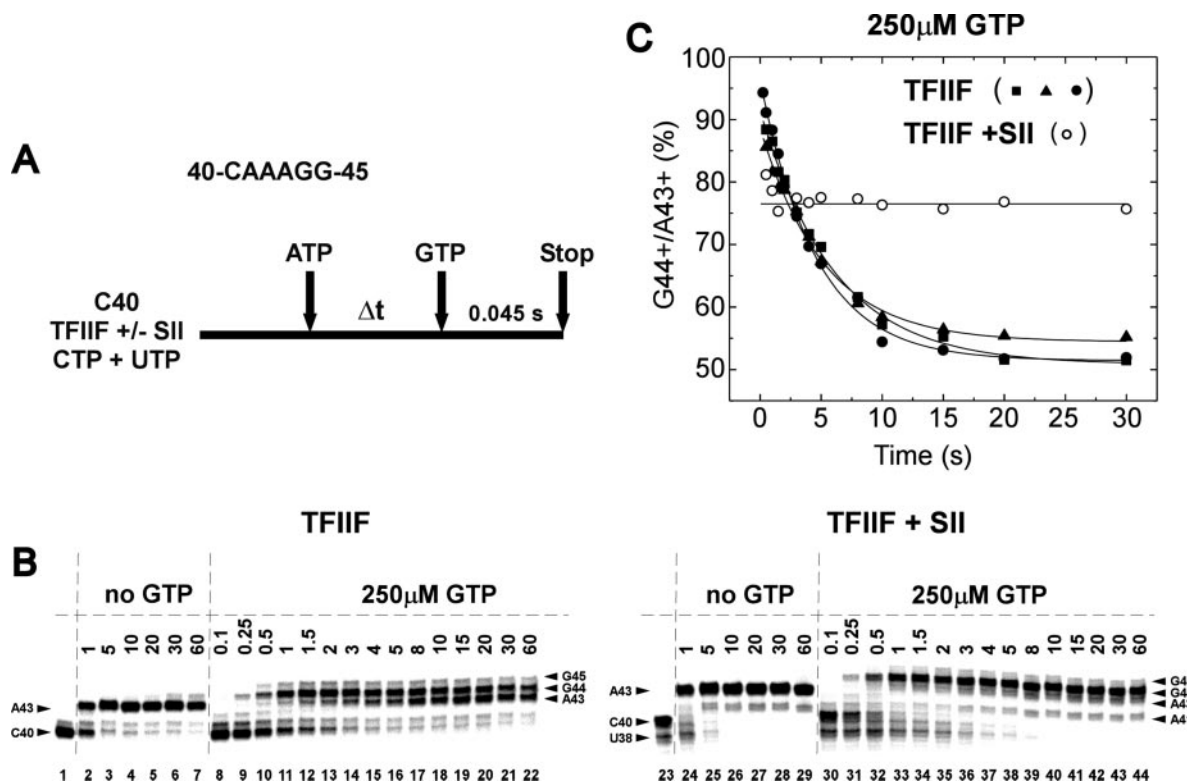


**FIG. 3. Combinatorial suppression of pausing by TFIIF and SII.** *A*, reaction protocol and RNA sequence. ECs were extended to the A43 position for different times followed by a 0.045-s chase with 250  $\mu$ M GTP. *B*, TFIIF-stimulated elongation in the absence of SII (*left panel*) (250  $\mu$ M GTP). *Lanes 1 and 23*, no ATP pulse, no GTP chase; *lanes 2–7 and 24–29*, 50  $\mu$ M ATP pulse and no GTP chase; *lanes 8–22 and 30–44*, 50  $\mu$ M ATP pulse and 250  $\mu$ M GTP chase for 0.045 s. *C*, plot of elongation efficiency percent versus ATP pulse time. Rates for equilibration of the active and the paused states are  $k_e = 0.19 \pm 0.01$ ,  $0.18 \pm 0.01$ , and  $0.21 \pm 0.01$  s $^{-1}$  in three independent experiments (Table I). In the presence of SII, the rate for equilibration of the active and paused states could not be measured.

ments, the efficiency calculation suffered slightly from inaccurate resolution on the time axis of the plots, as discussed above. Furthermore, rates of equilibration between the active synthesis and pausing pathways did not provide the rate constants for entry and exit from the pausing pathway ( $k_e = k_p + k_{-p}$ ). To re-enforce our conclusions and to obtain rate constants for pausing and exit from the paused state, we fit the data to kinetic models. These models are designed to account for rates of: 1) C40 disappearance, 2) entry into the paused state at A43, and 3) exit from the paused state at A43. As in the efficiency calculation, we assumed that all ECs detected at G44+, after the GTP chase, were in the A43a (active) state, and all ECs that remained at A43, after the GTP chase, were in the A43p (paused) state. Models are shown in Fig. 4 for the data obtained in the absence of SII and in Fig. 5 for the data obtained in the presence of SII. The results of these analyses complement and extend those based on the efficiency calculations and give insight into SII-mediated transcript cleavage.

To generate adequate simulations, a precise fit of the rate of C40 disappearance was required in order to obtain a consistent fraction of ECs advancing to downstream positions. Disappearance of C40 was modeled by a two-step process of C40a  $\rightarrow$  C40b  $\rightarrow$  A43, in which C40a and C40b represent different conformers of the C40 EC. In each case, a faster rate preceded a slower rate of C40 disappearance. We have not extensively analyzed the mechanism of C40 disappearance, so we do not know the best explanation for these two rates, except that multiple conformational steps may be required to escape the long term stall at C40. For the purposes of this paper, the precise mechanism of advance from C40 is not the most important issue, which relates to regulated escape from and pausing at A43. One observation, however, is particularly noteworthy. Escape from C40 is very slow and inefficient in the absence of

an elongation factor, compared with the presence of HDAG or TFIIF (compare Fig. 4, A–C), clearly demonstrating an important role for stimulatory elongation factors in escape from a long term stall. In the absence of an elongation factor, 73% of C40 ECs were active within the time course of the experiment. In the presence of HDAG, 92% of C40 ECs were observed to advance, and in the presence of TFIIF, 87% of C40 ECs advanced, demonstrating the importance of HDAG and TFIIF in elongation stimulation.

Because experiments were done with a single GTP chase time, we assumed that close to 100% of activated A43 ECs were extended to G44 and longer products, and close to 100% of paused ECs remained at A43 after the GTP chase. Based on prior experience, these assumptions are reasonable (5, 11). The distribution of A43a (active) and A43p (paused) states was determined as a function of stall time, as shown above. The data were fit to simple kinetic models, using the program KinTekSim (43, 44). We found, however, that kinetic models required an unexpected feature. Some fraction of ECs appeared to access the pausing pathway directly, rather than to first pass through the active A43a EC. Therefore, the step C40b  $\rightarrow$  A43p was included in the models in addition to the expected C40b  $\rightarrow$  A43a  $\rightarrow$  A43p pathway. The interpretation of the C40b  $\rightarrow$  A43p step in the model is that the deeply paused state can be accessed rapidly and directly during elongation by a fraction of ECs. Without this feature in the models, rates into and out of the paused state are too rapid to fit other experimental observations, or in some cases, the data cannot be fit at all. Inclusion of the C40b  $\rightarrow$  A43p step in pausing models is reviewed in more detail under the “Discussion.”

*Consistency of Kinetic Models with Efficiency Calculations*—From kinetic models, the rate constants into and out of the deeply paused EC are consistent with those obtained from the

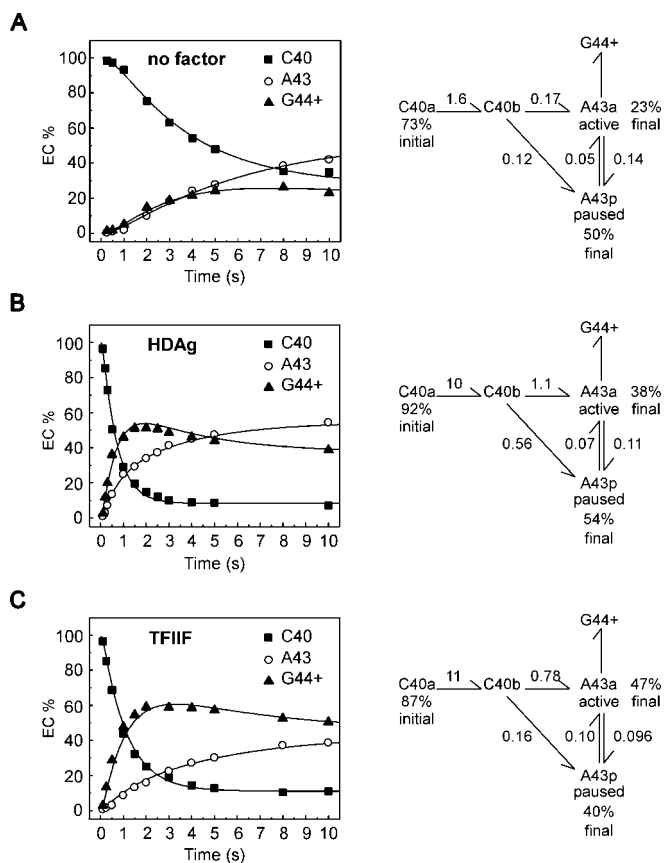


**FIG. 4. Regulation of RNAP II pausing by HDAG and TFIIF.** A, RNAP II pausing in the absence of a stimulatory elongation factor. B, RNAP II pausing in the presence of HDAG. This experiment was done with a 0.15-s GTP chase time, unlike the experiments shown in Fig. 2, which were done with a 0.045-s GTP chase time. C, RNAP II pausing in the presence of TFIIF. PhosphorImager quantitation of gel bands is shown to the left, and the corresponding kinetic model is shown to the right (see Figs. 1–3). The active fraction of C40 ECs (C40a) is indicated in percent. Occupancy of A43a is indicated by extension to G44 plus longer products (G44+). Paused A43 ECs (A43p) are those that remain at the A43 position after the GTP chase. The final fractions of A43a (active) and A43p (paused) are indicated in percent. Rate constants are given in units of  $s^{-1}$ . No ATP- or GTP-dependent steps are considered in these models.

efficiency calculations (Figs. 1–3; Table I). In the absence of a stimulatory factor (Fig. 1), the rate of equilibration between the active and paused states was  $0.20 s^{-1}$ , estimated from the efficiency calculation. As discussed above, this apparent rate should equal the sum of the rate constants into and out of the paused EC ( $k_e = k_p + k_{-p}$ ), and, therefore,  $0.2 \sim 0.14 + 0.05 s^{-1}$ , indicating that rate constants derived from the model are consistent with the efficiency calculation. In the presence of HDAG (Fig. 2), the rate of equilibration between the active and paused ECs was  $0.30 s^{-1}$ , from the efficiency calculation. Note that  $0.3 \sim 0.11 + 0.07 s^{-1}$ . Poorer agreement in the values for the reaction with HDAG can probably be attributed to the faster rate for the step  $C40b \rightarrow A43p$  ( $0.56$  versus  $0.12 s^{-1}$ ; compare Fig. 4, B and A). In the presence of TFIIF (Fig. 3), the rate of equilibration between the active and paused states was  $0.20 s^{-1}$ , estimated from the efficiency calculation. Note that  $0.2 \sim 0.096 + 0.1 s^{-1}$ . We conclude that the rate constants and models in Fig. 4 are adequate to describe the exit from the active synthesis pathway into the pausing pathway and show reasonable consistency with the efficiency calculations. Based on these models, HDAG and TFIIF do not appear to stimulate elongation by blocking the rate of exit into the paused EC. HDAG and TFIIF appear to stimulate elongation further along the active synthesis pathway.

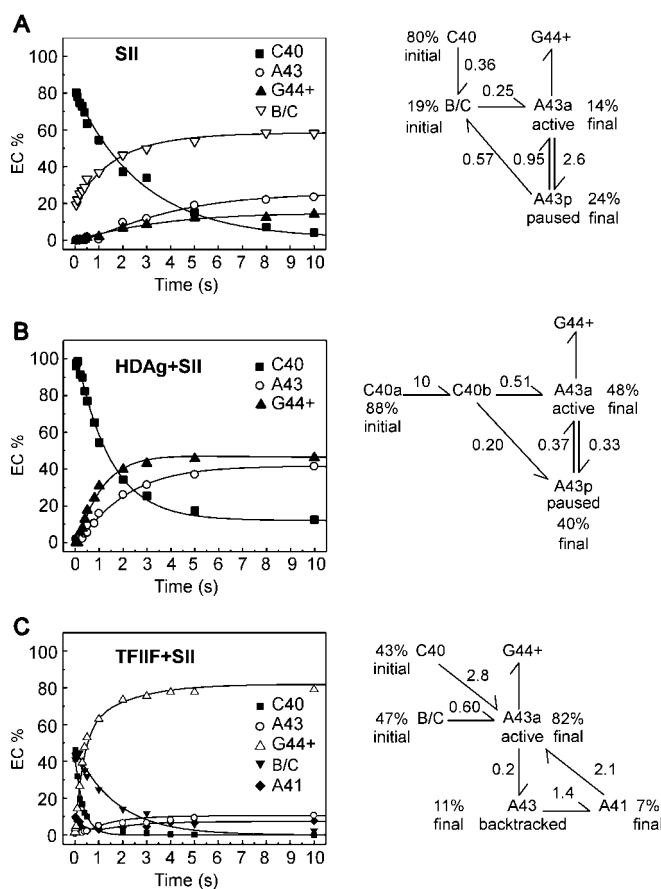


**FIG. 5. Combinatorial regulation of RNAP II pausing and transcript cleavage by TFIIF, HDAG, and SII.** A, RNAP II pausing and transcript cleavage in the presence of SII. B, RNAP II pausing and transcript cleavage in the presence of HDAG and SII. C, RNAP II pausing and transcript cleavage in the presence of TFIIF and SII. The experiment shown in C was done with a 0.150-s GTP chase time, in contrast to the experiments shown in Fig. 3, which were done with a 0.045-s GTP chase time. PhosphorImager quantitation of gel bands is shown to the left, and the corresponding kinetic model is shown to the right (see Figs. 1–3). The initial active fraction of C40 ECs (C40 or C40a) is indicated in percent. B and C indicates backtracked and cleaved ECs (primarily U38 and A41). Occupancy of A43a is indicated by efficient extension to G44 plus longer products (G44+). Paused A43 ECs (A43p) are those that remain at the A43 position after the GTP chase. C, A43 ECs that do not advance are interpreted to be backtracked rather than paused, because these ECs primarily appear to advance through cleavage to A41 (see Fig. 6). The final fractions of A43a, A43p, A43 (backtracked), and A41 are indicated in percent. A, A41 ECs are included in B and C. Rate constants are given in units of  $s^{-1}$ . No ATP- or GTP-dependent steps are considered in these models.

*Regulation of Transcript Cleavage and Pause Suppression by SII*—Fig. 5 shows kinetic modeling of reactions in the presence of SII. In the absence of an additional stimulatory elongation factor: 1) SII allows pausing at A43; 2) SII may accelerate rates into and out of the pausing pathway at A43; and 3) SII strongly stimulates transcript cleavage (Fig. 5A). Above, we estimated a minimal rate of  $>1.7 s^{-1}$  for the rate of equilibration (Fig. 1). From the kinetic model the rate constant from  $A43a \rightarrow A43p$  is estimated as  $2.6 s^{-1}$ , and the rate constant from  $A43p \rightarrow A43a$  is estimated as  $0.95 s^{-1}$ . Note that  $1.7 < 2.6 + 0.95 s^{-1}$ , as expected (Table I). Thus, SII appears to stimulate rates into and out of the paused A43 EC, although this observation could be attributed in part to the stimulation of transcript cleavage. Because SII stimulates backtracking and cleavage of RNA during the stall at A43, the true stall time at A43 may be shorter in the presence of SII than in its absence. SII strongly stimulates transcript cleavage, as indicated by the estimated rate

constant for A43p→A41 and shorter positions ( $0.57 \text{ s}^{-1}$ ). Also, under this condition, escape from C40 appears to occur mostly through SII-mediated cleavage from C40→U38 (Fig. 1B, right panel). As indicated from the accumulation of cleaved ECs, in the absence of HDAG and TFIIF, the stalled A43 EC appears to be losing the competition between transcript cleavage and forward synthesis, even in the presence of  $200 \mu\text{M}$  ATP (Fig. 1B, right panel). After cleavage, the EC may initially be in a conformation that cannot utilize NTPs (see “Discussion”).

In the presence of HDAG, SII-mediated transcript cleavage is strongly inhibited. Furthermore, SII appears to accelerate rates into and out of the paused EC ( $0.33$  versus  $0.11 \text{ s}^{-1}$  and  $0.37$  versus  $0.07 \text{ s}^{-1}$ ; compare Figs. 5B and 4B; Table I). Note that  $0.64 \sim 0.33 + 0.37 \text{ s}^{-1}$ , as expected, indicating reasonable consistency between efficiency calculations and kinetic models.

In the presence of TFIIF, SII has a profound effect on pausing, such that the paused A43 EC was not detected except as a probable intermediate in A43→A41 RNA cleavage (Fig. 5C). As indicated in Fig. 3, the rate of equilibration between the active and paused EC is rapid in the presence of both TFIIF and SII. For the experiment shown in Fig. 5C, the GTP chase time was  $0.15 \text{ s}$  rather than  $0.045 \text{ s}$ , to try to fully resolve paused from active pathway A43 ECs. Otherwise, the protocols are the same in Figs. 5C and 3. About 11% of ECs remain at A43 after the  $0.15\text{-s}$  GTP chase, and their rate of advancement is very similar to that of cleaved A41 ECs. Therefore, ECs remaining at A43 after the  $0.15\text{-s}$  GTP chase may be backtracked and largely committed to the A43→A41 cleavage pathway.

To gain more insight into pausing and transcript cleavage in the presence of TFIIF and SII, we performed the experiment shown in Fig. 6. For this experiment, a constant ATP pulse time of  $30 \text{ s}$  was followed by a variable chase time ( $0\text{--}5 \text{ s}$ ) with  $250 \mu\text{M}$  GTP. The protocol is shown at the top of the figure, and gel data are shown in Fig. 6A. In Fig. 6B we show the rate curve for G44+ synthesis with a  $0.1\text{-}$  or  $5\text{-s}$  time scale. For the  $0.1\text{-s}$  time scale (left panel), data were fit to a double exponential curve, indicating two rapid forward elongation rates. For the  $5\text{-s}$  time scale (right panel), the data were fit to a triple exponential curve, indicating three forward elongation rates, two rapid rates and a much slower rate. The three reaction phases have estimated rates of  $1400$  or  $1250$ ,  $31$  or  $37$ , and  $1.5 \text{ s}^{-1}$  and occupancies of  $39$ ,  $43$ , or  $41$  and  $24\%$  of total ECs. A41, which is generated by SII-mediated RNA cleavage from A43, accounts for  $14\%$  of total ECs and is included in the  $24\%$  of slowest phase ( $1.5 \text{ s}^{-1}$ ) ECs. In Fig. 6C, we show an adequate kinetic model to describe escape from A43 in the presence of TFIIF and SII. The view that emerges is that faster and slower phases ( $1250$  and  $33 \text{ s}^{-1}$  rates) represent different conformations of the active A43 EC. Previously, we interpreted A43a2 and A43a1 ECs as differing in their initial translocation state: the fastest phase ( $1250 \text{ s}^{-1}$ ) being post-translocated and the slower phase ( $33 \text{ s}^{-1}$ ) being pretranslocated (5). The slowest phase of A43 EC ( $2 \text{ s}^{-1}$ ,  $7\%$  occupancy) we interpret primarily as backtracked but not yet cleaved to A41. These A43 ECs appear to advance primarily through SII-mediated cleavage to A41 followed by slow escape ( $2 \text{ s}^{-1}$ ) from A41→G44+. The slow rate of disappearance from A43→A41 indicates that SII-mediated cleavage is slow but faster than conversion of the backtracked A43 EC to the active A43 EC (A43(backtracked)→A43a1 is slow compared with A43(backtracked)→A41).

We conclude that cellular elongation factors TFIIF and SII cooperate to suppress pausing by accelerating rates out of and perhaps into the pausing pathway. Furthermore, TFIIF adjusts the EC for forward elongation, resisting stimulation of backtracking by SII. Essentially, in the presence of TFIIF and SII, the pausing pathway merges with the active synthesis

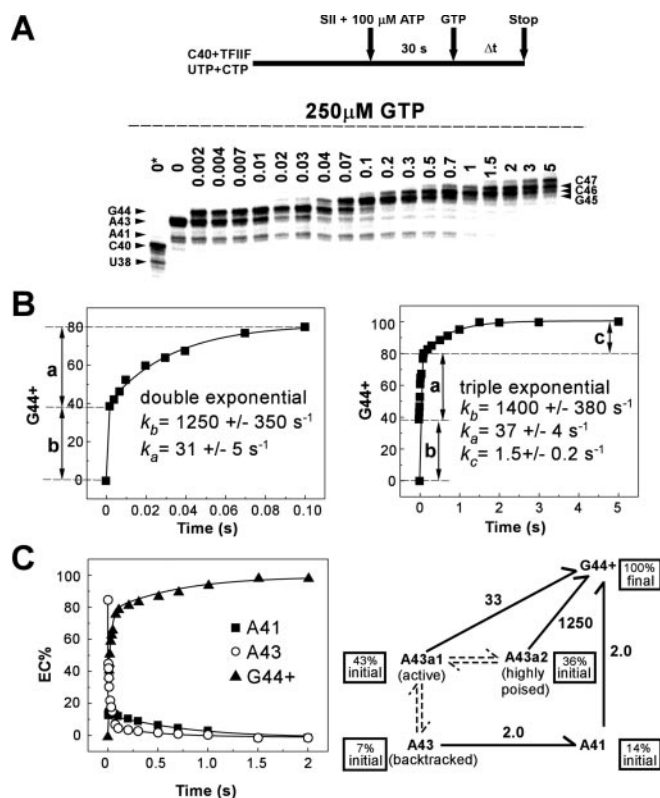


**FIG. 6. Combinatorial suppression of transcriptional pausing by TFIIF and SII.** The protocol is at the top of the figure. A, gel data. The ATP pulse was for  $30 \text{ s}$ . GTP chase times are given in seconds.  $0^*$  indicates no ATP pulse and no GTP chase. During the GTP chase, the concentrations of NTPs were  $250 \mu\text{M}$  GTP,  $50 \mu\text{M}$  ATP,  $5 \mu\text{M}$  CTP, and  $5 \mu\text{M}$  UTP. B and C, PhosphorImager quantitation and simulation of the data shown in A. B, model-independent analysis. A very fast rate and a somewhat slower rate of A43→G44+ elongation are detected within  $0.1 \text{ s}$  (left panel), and an additional very slow rate is detected within  $5 \text{ s}$  (right panel). The rates and fractional occupancies of these EC states are as follows: for A43a2 (active, highly poised),  $k_b = 1250 \pm 350$  or  $1400 \pm 380 \text{ s}^{-1}$ , occupancy =  $39 \pm 2\%$ ; for A43a1 (active),  $k_a = 31 \pm 5$  or  $37 \pm 4 \text{ s}^{-1}$ , occupancy =  $43 \pm 2$  or  $40 \pm 2\%$ ; and for A43 (backtracked) and A41,  $k_c = 1.5 \pm 0.2 \text{ s}^{-1}$ , occupancy =  $24 \pm 2\%$ . A43a2 and A43a1 represent distinct conformations of the active A43 EC poised to elongate at different rates (5). Rates estimated from the model-independent analysis (B) were the basis for the simulation shown in C.

pathway. The pausing pathway must be maintained, because the paused EC is the logical entry into the backtracked A43 EC, which is the substrate for A43→A41 cleavage. Viral elongation factor HDAG does not cooperate with SII to suppress transcriptional pausing. Rather, HDAG appears to antagonize SII-mediated transcript cleavage, indicating that the paused EC that HDAG supports may not be sufficiently backtracked to provide a substrate for SII-stimulated cleavage. These observed differences between TFIIF and HDAG in the regulation of pausing and SII-mediated transcript cleavage are consistent with the observation that TFIIF and HDAG regulate RNAP II elongation in distinct ways (5).

## DISCUSSION

**Combinatorial Regulation of Pausing and Transcript Cleavage**—To explain combinatorial effects of HDAG, TFIIF, and SII on transcriptional pausing and transcript cleavage, we offer the models shown in Fig. 7. Fig. 7, A and B, shows the main elongation pathways for HDAG- and TFIIF-stimulated elongation and divergence from the active pathway into the pausing pathway (5). For the HDAG-stimulated mechanism, the pretranslocated state appears to be on-line during rapid synthesis. For the TFIIF-stimulated mechanism, however, the apparent

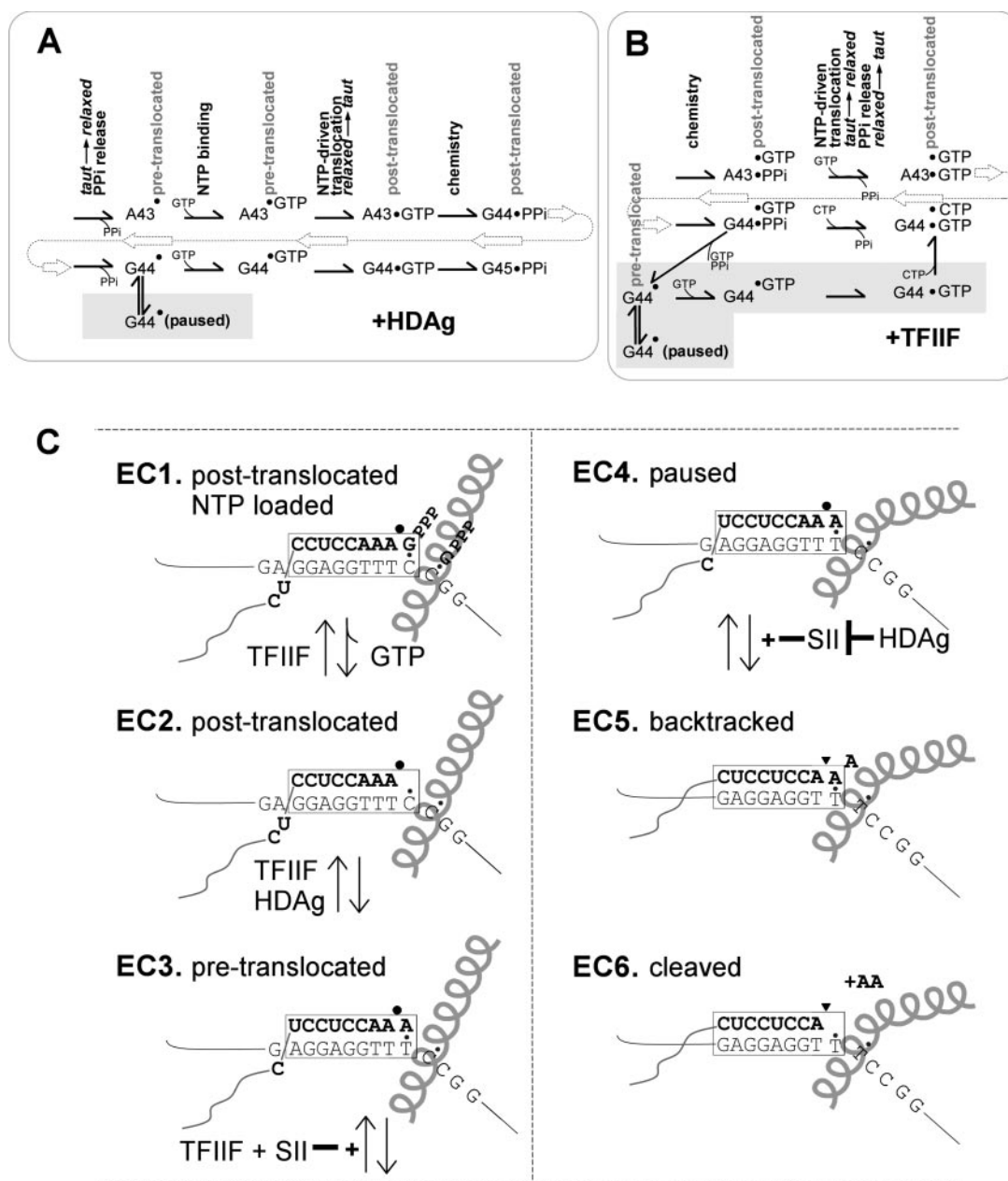


FIG. 7. Regulation of RNAP II elongation and the branch into the pausing and RNA cleavage pathway. A, HDAG-stimulated mechanism, main elongation pathway and branch to the pausing pathway (shaded in gray). B, TFIIF-stimulated mechanism, main elongation pathway and branch to the pausing pathway and an off-line elongation pathway (shaded in gray). C, states of the RNAP II EC indicated in this work. The position of the bridge  $\alpha$ -helix next to the RNAP II active site (represented by a black dot or triangle (in RNA cleavage mode)) is shown. Bending of the bridge helix is meant to indicate a conformational change in RNAP II associated with pausing. The box surrounding the 8–9-bp RNA-DNA hybrid represents the RNAP II clamp, which prefers to hold a 9-bp hybrid (47, 48). RNA and NTPs are indicated in boldface. The DNA template is indicated in lightface type.

coupling of NTP-driven translocation to pyrophosphate release places the pretranslocated state off-line during the most rapid RNA synthesis (compare Fig. 7, A and B). In both models, the pretranslocated EC connects directly to the paused EC.

In Fig. 7C, we show multiple states on the pausing pathway, indicated from this study and previous work (5). EC1 represents the post-translocated EC in the presence of NTPs. In accordance with the NTP-driven translocation model, both the  $n + 1$  and  $n + 2$  GTPs ( $n = \text{RNA length}$ ) are paired with their cognate DNA bases (5). EC2 represents the post-translocated EC in the absence of NTPs. In Fig. 6, the highly poised A43a2 EC is thought to correspond to the post-translocated EC2 (5). In EC2 the clamp holds an 8-bp RNA-DNA hybrid rather than the preferred 9-bp hybrid (47, 48). Because of the shortened hybrid

in EC2, elongation factors, such as HDAG and TFIIF, are required to stabilize the post-translocated EC. Stabilization of poised ECs by stimulatory elongation factors has been noted by others (49, 50). As the post-translocated EC2 reverts to the pretranslocated EC3, the 9-bp hybrid is re-established. In Fig. 6, the slower A43a1 EC is thought to correspond to the pretranslocated EC3. The added stability that arises from filling the clamp with a 9-bp hybrid probably explains why the yeast RNAP II EC structure was visualized primarily in the pretranslocated conformation (47, 48). EC4 represents the paused EC. EC4 must be distinct from EC3 in conformation, because EC3 elongation is rapid, and EC4 elongation is very slow (4, 5, 11). We propose, however, that EC4 is pretranslocated but not further backtracked, because, in the presence of HDAG and SII,

the paused EC4 is resistant to SII-mediated RNA cleavage (Figs. 2 and 5B). In Fig. 7C, we indicate the conformational change in EC4 by introducing a bend in the bridge  $\alpha$ -helix, although we do not know what structural change in RNAP II accompanies the EC3→EC4 transition. EC5 represents the backtracked, SII-sensitive EC. Evidence for EC5 is abundant in Figs. 1B (right panel), 3B (right panel), 5, A and C, and 6, which show significant evidence of SII-stimulated dinucleotide cleavage. EC6 represents the EC conformation after cleavage and release of the pApA dinucleotide (A43→A41).

Backtracking by one nucleotide from the pretranslocated state positions the RNAP II active site for cleavage of a dinucleotide, the preferred SII-mediated cleavage product under elongation conditions (27, 28, 35, 38). If SII were to stimulate mononucleotide cleavage, the pretranslocated EC3 might be sensitive to SII-mediated cleavage, which would merge the RNA synthesis and the RNA cleavage pathways, at least for some modes of elongation (*i.e.* HDag-stimulated elongation; Fig. 7A). Multisubunit RNAPs, therefore, may have evolved to cleave nascent RNA in dinucleotide rather than mononucleotide increments, to move RNA cleavage further off-line from ongoing synthesis. Backtracked ECs are most evident in the presence of SII as the sole elongation factor, in which case SII-mediated cleavage is very aggressive (Fig. 1). When HDag and TFIIF are absent, the EC readily reverts to deeply paused forms that are highly sensitive to SII-mediated cleavage, and SII may stimulate backtracking in these unprotected RNAP II ECs, in addition to stimulating RNA cleavage. In the presence of both TFIIF and SII, EC5 and EC6 are detected as A43→A41 cleavage, although only a small fraction of A43 ECs proceed through the RNA cleavage pathway.

In the presence of HDag or TFIIF, the EC appears to resist SII-mediated cleavage by maintaining more highly poised conformations for elongation. TFIIF and SII combine to suppress pausing by RNAP II. HDag maintains the EC to resist SII-mediated cleavage but does not cooperate with SII to suppress pausing. Both TFIIF and HDag support elongation modes that insulate the active synthesis path from the pausing and RNA cleavage path, and pause suppression by these elongation factors is therefore maintained further along the active elongation pathway than at the branch into the paused EC.

In the presence of SII, dinucleotide cleavage products are slow to recover. Because a recovery period is necessary before rapid synthesis can resume, a slow conformational change must occur before these ECs can re-enter the active synthesis pathway (Fig. 7C). The conformation of EC6 (after SII-induced cleavage) resembles paused EC4, rather than ECs1–3 on the active elongation pathway. Slow recovery of edited RNAs in the presence of SII may explain why, in the absence of HDag and TFIIF, SII cleavage of the RNAP II EC is so aggressive (Fig. 1). Because RNA cleavage is expected to result in EC6, if other elongation factors are absent, SII might be expected to stimulate further backtracking and cleavage before the EC could recover to a conformation capable to utilize NTPs and resume forward synthesis.

*Evidence for Two Routes of Entry into the Paused EC*—During transcriptional stalling, entry of RNAP II ECs onto the pausing pathway is observed to be too fast to be accounted for, if all paused ECs are formed from active ECs at the stall position. Because of this observation, in Figs. 4 and 5B a step was included in kinetic models, such that the paused EC was on-line for a fraction of ECs approaching the stall position at A43 (C40b→A43p, in addition to C40b→A43a→A43p). Including this additional step allowed consistency between kinetic models (Figs. 4 and 5B) and efficiency calculations (Figs. 1–3), as discussed under “Results.” By using a kinetic model that

lacks the C40b→A43p step, the data in Fig. 4B could not be fit, because paused A43 ECs appear too rapidly. The data sets in Figs. 4, A and C, and 5B can be fit to a model lacking the C40b→A43p step, but rate constants into and out of the paused EC are too fast to be consistent with other data. There are two problems with kinetic models that lack a direct route from the active synthesis into the pausing pathway (C40b→A43p): 1) rate constants are too fast to be consistent with efficiency calculations; and 2) rate constants out of the pausing pathway (A43p→A43a) are too fast to be consistent with previous measurements (5). In the presence of HDag, the rate constant for A43p→A43a was previously estimated as  $0.05\text{ s}^{-1}$ , and in the presence of TFIIF, this rate constant was estimated as  $0.09\text{ s}^{-1}$  (5). We have reexamined these data to obtain the best possible determinations of these rate constants, using model-independent analysis (see “Experimental Procedures”). Estimations of the value for  $k_{-p}$  come from the rate of the slowest reaction phase of the forward reaction from A43 at high GTP concentration. Under this condition, the slowest rate of the forward reaction is limited by the rate of escape from the paused EC, yielding an estimate of  $k_{-p}$  (5). Our best estimates for these values are  $k_{-p} = 0.04$  to  $0.06\text{ s}^{-1}$  (no factor),  $k_{-p} = 0.066 \pm 0.002\text{ s}^{-1}$  (HDag), and  $k_{-p} = 0.10 \pm 0.012\text{ s}^{-1}$  (TFIIF). In this paper, we report these rates as 0.05 (no factor), 0.07 (HDag), and  $0.10\text{ s}^{-1}$  (TFIIF), very close to our best estimates. The close correspondence of these numbers indicates that the kinetic models that we report are adequate to fit experimental data. Furthermore, we conclude from this analysis that a fraction of RNAP II ECs is likely to test the pausing pathway at A43 without first passing through the A43a state. Thus, the paused A43p EC appears to be on-line for a fraction of ECs during rapid elongation, indicating that some RNAP II ECs pause at every base position, whether or not it is a preferred pause site. Because the A43 position is not a natural pause position (data not shown), we believe that at many or all base positions some fraction of ECs will diverge into the paused state before continuing on the active pathway.

*A Role for SII in Pause Suppression*—We show here that TFIIF and SII cooperate to suppress RNAP II pausing, significantly improving the efficiency of elongation after a brief transcriptional stall. Although transcript cleavage induced by SII may contribute to stall recovery, pause suppression appears primarily to be a combinatorial effect of TFIIF and SII to merge the pausing pathway with the active synthesis pathway, so that stably paused ECs are not apparent in the presence of both factors. Thus, in combination with TFIIF, SII appears to have a transcriptional activity that does not require RNA cleavage and that is closer to the active RNA synthesis pathway than the cleavage and restart reaction. SII does not stimulate overall elongation rates, either in the presence or absence of TFIIF, at high (6, 7) or low (data not shown) NTP concentrations. Readthrough of arrest sites has been monitored as an SII function (51–55). Some SII mutants with moderate RNA cleavage activity do not appear to stimulate readthrough, indicating that stimulating transcript cleavage may not be the sole function of SII (51, 52). To our knowledge, ours is the first report of combinatorial suppression of pausing by SII and TFIIF and the first report that SII (with TFIIF) may be an allosteric regulator of RNAP II pausing. The assay we have developed will allow a reassessment of SII mutant proteins to identify lesions that may separate cleavage from pause suppression activities. By analogy, the GreA and GreB factors of bacteria, which are functional analogues of human SII, could have similar allosteric roles in regulating pausing by bacterial RNAP.

*SII as an Allosteric Effector of RNAP II*—The recent x-ray crystal structure of yeast RNAP II bound to yeast SII (domains

II and III) indicates that SII may be an allosteric effector of RNAP II (37), as indicated by our kinetic studies. SII binding induces many changes in RNAP II conformation, including alterations expected to affect RNAP II catalysis. Domain II of SII binds the Rpb1 subunit “jaw” of RNAP II, which helps to hold the incoming downstream DNA in the EC. An interdomain linker extends from SII domain II to domain III and restructures RNAP II regions with which it interacts. SII domain III is a  $Zn^{2+}$  finger that penetrates the RNAP II “pore,” a solvent entry to the RNAP II active site. The tip of the SII (domain III)  $Zn^{2+}$  finger carries a conserved Asp-Glu motif, thought to chelate a  $Mg^{2+}$  atom that participates in RNA cleavage. SII affects the structure of the “trigger” loop underlying the “bridge”  $\alpha$ -helix, inducing movement of the bridge helix. In the EC, the bridge helix touches the RNA-DNA hybrid at the 3' end of the growing RNA chain, so the bridge helix is thought to be important in translocation (5, 47). SII binding reorients “switch 1” and “switch 2” outward from positions where these peptide chains would grasp the RNA-DNA hybrid in the EC. SII binding, therefore, might be expected to promote motion and possibly translocation of the RNA-DNA hybrid, consistent with our observation that human SII and TFIIF cooperate to suppress transcriptional pausing by RNAP II. Freer movement of the RNA-DNA hybrid could facilitate the conformational change between the paused EC4 and the pretranslocated EC3 (Fig. 7C).

**Acknowledgments**—We thank Y. A. Nediaikov and X. Q. Gong of our laboratory for help with many aspects of this project. We gratefully acknowledge Y. Yamaguchi for the HDAG clone.

## REFERENCES

- Johnson, K. A. (1993) *Annu. Rev. Biochem.* **62**, 685–713
- Johnson, K. A. (1992) *Enzymes* **20**, 1–61
- Johnson, K. A. (1995) *Methods Enzymol.* **249**, 38–61
- Nediaikov, Y. A., Gong, X. Q., Yamaguchi, Y., Handa, H., and Burton, Z. F. (2003) *Methods Enzymol.* **371**, 252–262
- Nediaikov, Y. A., Gong, X. Q., Hovde, S. L., Yamaguchi, Y., Handa, H., Geiger, J. H., Yan, H., and Burton, Z. F. (2003) *J. Biol. Chem.* **278**, 18303–18312
- Bengal, E., Flores, O., Krauskopf, A., Reinberg, D., and Aloni, Y. (1991) *Mol. Cell. Biol.* **11**, 1195–1206
- Izban, M. G., and Luse, D. S. (1992) *J. Biol. Chem.* **267**, 13647–13655
- Tan, S., Aso, T., Conaway, R. C., and Conaway, J. W. (1994) *J. Biol. Chem.* **269**, 25684–25691
- Ren, D., Lei, L., and Burton, Z. F. (1999) *Mol. Cell. Biol.* **19**, 7377–7387
- Lei, L., Ren, D., and Burton, Z. F. (1999) *Mol. Cell. Biol.* **19**, 8372–8382
- Funk, J. D., Nediaikov, Y. A., Xu, D., and Burton, Z. F. (2002) *J. Biol. Chem.* **277**, 46998–47003
- Renner, D. B., Yamaguchi, Y., Wada, T., Handa, H., and Price, D. H. (2001) *J. Biol. Chem.* **276**, 42601–42609
- Lai, M. M. (1995) *Annu. Rev. Biochem.* **64**, 259–286
- Taylor, J. M. (1999) *Curr. Top. Microbiol. Immunol.* **239**, 107–122
- Taylor, J. M. (2003) *Trends Microbiol.* **11**, 185–190
- Jeng, K. S., Su, P. Y., and Lai, M. M. (1996) *J. Virol.* **70**, 4205–4209
- Huang, Z. S., and Wu, H. N. (1998) *J. Biol. Chem.* **273**, 26455–26461
- Yamaguchi, Y., Filipovska, J., Yano, K., Furuya, A., Inukai, N., Narita, T., Wada, T., Sugimoto, S., Konarska, M. M., and Handa, H. (2001) *Science* **293**, 124–127
- Yamaguchi, Y., Delehouzee, S., and Handa, H. (2002) *Microbes Infect.* **4**, 1169–1175
- Fu, T. B., and Taylor, J. (1993) *J. Virol.* **67**, 6965–6972
- Modahl, L. E., Macnaughton, T. B., Zhu, N., Johnson, D. L., and Lai, M. M. (2000) *Mol. Cell. Biol.* **20**, 6030–6039
- Chang, J., and Taylor, J. (2002) *EMBO J.* **21**, 157–164
- Filipovska, J., and Konarska, M. M. (2000) *RNA (New York)* **6**, 41–54
- Reines, D., Ghanouni, P., Li, Q. Q., and Mote, J., Jr. (1992) *J. Biol. Chem.* **267**, 15516–15522
- Reines, D. (1992) *J. Biol. Chem.* **267**, 3795–3800
- Wang, D., and Hawley, D. K. (1993) *Proc. Natl. Acad. Sci. U. S. A.* **90**, 843–847
- Izban, M. G., and Luse, D. S. (1992) *Genes Dev.* **6**, 1342–1356
- Guo, H., and Price, D. H. (1993) *J. Biol. Chem.* **268**, 18762–18770
- Wind, M., and Reines, D. (2000) *BioEssays* **22**, 327–336
- Koulich, D., Orlova, M., Malhotra, A., Sali, A., Darst, S. A., and Borukhov, S. (1997) *J. Biol. Chem.* **272**, 7201–7210
- Kulish, D., Lee, J., Lomakin, I., Nowicka, B., Das, A., Darst, S., Normet, K., and Borukhov, S. (2000) *J. Biol. Chem.* **275**, 12789–12798
- Koulich, D., Nikiforov, V., and Borukhov, S. (1998) *J. Mol. Biol.* **276**, 379–389
- Powell, W., Bartholomew, B., and Reines, D. (1996) *J. Biol. Chem.* **271**, 22301–22304
- Rudd, M. D., Izban, M. G., and Luse, D. S. (1994) *Proc. Natl. Acad. Sci. U. S. A.* **91**, 8057–8061
- Gu, W., and Reines, D. (1995) *J. Biol. Chem.* **270**, 30441–30447
- Opalka, N., Chlenov, M., Chacon, P., Rice, W. J., Wriggers, W., and Darst, S. A. (2003) *Cell* **114**, 335–345
- Kettenberger, H., Armache, K. J., and Cramer, P. (2003) *Cell* **114**, 347–357
- Izban, M. G., and Luse, D. S. (1993) *J. Biol. Chem.* **268**, 12874–12885
- Izban, M. G., and Luse, D. S. (1993) *J. Biol. Chem.* **268**, 12864–12873
- Shapiro, D. J., Sharp, P. A., Wahli, W. W., and Keller, M. J. (1988) *DNA (New York)* **7**, 47–55
- Wang, B. Q., Kostrub, C. F., Finkelstein, A., and Burton, Z. F. (1993) *Protein Expression Purif.* **4**, 207–214
- Wang, B. Q., Lei, L., and Burton, Z. F. (1994) *Protein Expression Purif.* **5**, 476–485
- Barshop, B. A., Wrenn, R. F., and Frieden, C. (1983) *Anal. Biochem.* **130**, 134–145
- Zimmerle, C. T., and Frieden, C. (1989) *Biochem. J.* **258**, 381–387
- Foster, J. E., Holmes, S. F., and Eerie, D. A. (2001) *Cell* **106**, 243–252
- Dunlap, C. A., and Tsai, M. D. (2002) *Biochemistry* **41**, 11226–11235
- Gnatt, A. L., Cramer, P., Fu, J., Bushnell, D. A., and Kornberg, R. D. (2001) *Science* **292**, 1876–1882
- Gnatt, A. (2002) *Biochim. Biophys. Acta* **1577**, 175–190
- Gu, W., and Reines, D. (1995) *J. Biol. Chem.* **270**, 11238–11244
- Elmendorf, B. J., Shilatifard, A., Yan, Q., Conaway, J. W., and Conaway, R. C. (2001) *J. Biol. Chem.* **276**, 23109–23114
- Cipres-Palacin, G., and Kane, C. M. (1994) *Proc. Natl. Acad. Sci. U. S. A.* **91**, 8087–8091
- Cipres-Palacin, G., and Kane, C. M. (1995) *Biochemistry* **34**, 15375–15380
- Ubukata, T., Shimizu, T., Adachi, N., Sekimizu, K., and Nakanishi, T. (2003) *J. Biol. Chem.* **278**, 8580–8585
- Fish, R. N., and Kane, C. M. (2002) *Biochim. Biophys. Acta* **1577**, 287–307
- Jeon, C., Yoon, H., and Agarwal, K. (1994) *Proc. Natl. Acad. Sci. U. S. A.* **91**, 9106–9110